ISSN 1674-1056
http://cpb.iphy.ac.cn
http://iopscience.iop.org/cpb
中国物理 B
Chinese Physics
中国物理 Chinese Physics B

Random phase screen influence of the inhomogeneous tissue layer on the generation of acoustic vortices

Zhiyao Ma(马致遥), Jun Ma(马骏), Dong Zhang(章东), Juan Tu(屠娟)
Citation: Chin. Phys. B . 2018, 27(3): 034301. **doi:** 10.1088/1674-1056/27/3/034301

Journal homepage: http://cpb.iphy.ac.cn; http://iopscience.iop.org/cpb

What follows is a list of articles you may be interested in

Random phase screen influence of the inhomogeneous tissue layer on the generation of acoustic vortices

Zhiyao Ma(马致遥), Jun Ma(马骏), Dong Zhang(章东), Juan Tu(屠娟)
Chin. Phys. B . 2018, 27(3): 034301. **doi:** 10.1088/1674-1056/27/3/034301

Acoustic radiation force on a multilayered sphere in a Gaussian standing field

Haibin Wang(汪海宾), Xiaozhou Liu(刘晓宙), Sha Gao(高莎), Jun Cui(崔骏), Jiehui Liu(刘杰惠), Aijun He(何爱军), Gutian Zhang(张古田)
Chin. Phys. B . 2018, 27(3): 034302. **doi:** 10.1088/1674-1056/27/3/034302

Multiple off-axis acoustic vortices generated by dual coaxial vortex beams

Wen Li(李雯), Si-Jie Dai(戴思捷), Qing-Yu Ma(马青玉), Ge-Pu Guo(郭各朴), He-Ping Ding(丁鹤平)
Chin. Phys. B . 2018, 27(2): 024301. **doi:** 10.1088/1674-1056/27/2/024301

Acoustic radiation force induced by two Airy-Gaussian beams on a cylindrical particle

Sha Gao(高莎), Yiwei Mao(毛一葳), Jiehui Liu(刘杰惠), Xiaozhou Liu(刘晓宙)
Chin. Phys. B . 2018, 27(1): 014302. **doi:** 10.1088/1674-1056/27/1/014302

Array gain for a conformal acoustic vector sensor array: An experimental study

Yong Wang(汪勇), Yi-Xin Yang(杨益新), Zheng-Yao He(何正耀), Bo Lei(雷波), Chao Sun(孙超), Yuan-Liang Ma(马远良)
Chin. Phys. B . 2016, 25(12): 124318. **doi:** 10.1088/1674-1056/25/12/124318

Random phase screen influence of the inhomogeneous tissue layer on the generation of acoustic vortices*

Zhiyao Ma(马致遥)[1], Jun Ma(马骏)[2,†], Dong Zhang(章东)[3,‡], and Juan Tu(屠娟)[3]

[1] *Tsien Hsue-shen College, Nanjing University of Science and Technology, Nanjing* 210094, *China*
[2] *School of Electronic and Optical Engineering, Nanjing University of Science and Technology, Nanjing* 210094, *China*
[3] *Institute of Acoustics, Nanjing University, Nanjing* 210093, *China*

(Received 4 November 2017; revised manuscript received 1 December 2017; published online 11 February 2018)

The influence of the inhomogeneous tissue layer on the generation of acoustic vortices (AV) is studied theoretically and experimentally based on the phase screen model. By considering the time-shift of a random phase screen, the formula of acoustic pressure for the AV beam generated by a circular array of eight planar piston sources is derived. With the actual correlation length of the abdominal wall, numerical simulations before and after the insertion of the inhomogeneous tissue layer are conducted, and also demonstrated by experimental measurements. It is proved that, when the thickness variation of the phase screen is less than one wavelength, no significant influence on the generation of AVs can be produced. The variations of vortex nodes and antinodes in terms of the location, shape, and size of AVs are not obvious. Although the circular pressure distribution might be deformed by the phase interference with a larger thickness variation, AVs can still be generated around the center axis with perfect phase spirals in a reduced effective radius. The favorable results provide the feasibility of AV generation inside the human body and suggest the application potential of AVs in object manipulation for biomedical engineering.

Keywords: acoustic vortices, random phase screen, phase spiral, correlation length

PACS: 43.25.Qp, 43.60.Fg, 43.38.Hz **DOI:** 10.1088/1674-1056/27/3/034301

1. Introduction

After the concept of wave front dislocation[1] was introduced by Nye in 1974, the physical meaning of the phase dislocation or the phase singularity in wave propagation attracts more and more attention to the optical vortex (OA). Due to the characteristics of the polarization and the rotational angular momentum of light, the unique structure of phase in OAs was demonstrated to possess the orbital angular momentum (OAM), which could be used to manipulate objects with the exerted rotation torque. In 1992, driven by the OAM transferred from a Laguerre–Gaussian laser beam,[2] the particles were observed to rotate around the beam axis successfully. Through the experimental measurement of the torque, Allen also proved that the OAM of an OA was proportional to the corresponding topological charge. Then, the basic theory of OA was explained in detail by Neuma[3] and the structure design of optical tweezers was also proposed to improve the effects in optical manipulation.

Compared to the light beam, acoustic waves can propagate into deep media and can be used to manipulate particles inside tissues, which suggest the feasibility of broad applications in nondestructive testing and biomedical engineering. By using two sets of phased ultrasonic transducer arrays, the accurate position control of standing wave node[4] in air was realized by Hoshi and the practical application of three-dimensional (3-D) manipulation for mm-scale particles was also demonstrated. Then, based on the surface resonance of phononic crystals, an acoustic sieve[5] was designed by Li to locate, capture, sift and transport nanoscale particles with a local high radiation force. However, the application of the proposed methods is still hindered by the specific manner of the acoustic field.

As a kind of acoustic wave with continuous helical wave fronts around the beam axis, the acoustic vortex (AV)[6–8] shows an obvious pressure zero at the vortex center with an intrinsic phase singularity. The possibility of the OAM transfer to objects is produced by the continuous phase spiral. The object manipulation inside tissues can be realized by the exerted radiation torque, which shows significant application potential in biomedical and industrial areas. An underwater ultrasonic calibration system[9] composed of four high-frequency transducers was designed. The existence of screw wave fronts and phase dislocations was proved and the qualitative relationship between the acoustic pressure and the OAM of the AV was also obtained. A quantitative test[10] for the OAM transfer from the AV to an acoustic absorbing object immersed in a viscous liquid was conducted by Anhauser. In addition, Demore[11] proved that the ratio of the OAM to the acoustic power of an AV was equivalent to the ratio of the topological charge l to the angular frequency ω.

*Project supported by the National Natural Science Foundation of China (Grant Nos. 61575095, 11374155, and 11674173).
†Corresponding author. E-mail: majun@njust.edu.cn
‡Corresponding author. E-mail: dzhang@nju.edu.cn
© 2018 Chinese Physical Society and IOP Publishing Ltd

In order to generate AVs with sparse sources, a phase-coded approach[12] was proposed by Yang using a circular array of point sources. It was proved that, for N point sources, the AV beam with a controllable topological charge can be generated, and the phase difference resolution of the adjacent sources was demonstrated to be π. The maximum topological charge of the AV beam generated by an N-element system was proved to be fix$[(N-1)/2]$, where fix(x) rounded the element x towards zero. Then, the distributions of acoustic pressure and phase for AVs were studied by Gao[13] and Zheng,[14] and the judge criterion for linear circular phase distribution and the impact factors for annular pressure distribution were also proposed. Moreover, by considering the directivity of the sources, Li extended the point source model to a high-frequency directional source array.[15] Theoretical and experimental results showed that AVs could be generated by the main lobe and the side lobes of the directional sources along the beam axis. The vortex valleys (nodes) produced by the pressure nulls (PNs) between the lobes were located on the beam axis to form deep-level multiple traps, which provided the feasibility of 3D manipulation.

In previous studies, the generation of AVs was investigated only in a single medium without the consideration of acoustic transmission in layered or inhomogeneous media. However, the acoustic propagation can be influenced by the inhomogeneity of tissues, resulting in great impact on AVs. In biomedical applications, due to the layered structure and the inhomogeneity of tissues, the abdominal wall should not be treated as a single homogeneous medium. In the field of high-intensity focused ultrasound (HIFU) therapy, the layered model[16–18] of tissues was established to study the influence of layered media on the pressure distribution in the focal area; whereas, the structure of the model is different from that of the abdominal wall, and the phase distortion in acoustic propagation is sensitive[19,20] to the phased array in medical devices. It was reported by Liu that the inhomogeneity of the abdominal wall has obvious influences on the location, shape, and intensity of the focal region, and the impact of the phase distortion introduced by the time delay is more significant[21–23] than that caused by acoustic attenuation in tissues. For the phase-coded approach, besides the physical characteristics of the circular transducer array, the generation of AVs is determined by the accurate individual phase control for each source. Since the acoustic pressure at each point is the superimposition of the signals transmitted from the sources, the distribution of the AV will be affected by the phase shift during the acoustic transmission. Obvious location deviation and pressure deformation of AVs will be produced by the range of the random phase variation. Therefore, the influence of the inhomogeneous tissue layer should be taken into account on the generation of AVs, especially for the abdominal wall in human body.

In this paper, based on the phase variation of the abdominal wall, the influence of the inhomogeneous tissue layer on the generation of AVs is investigated using the random phase screen model. For the AV beam generated by a circular array of planar transducers, the inhomogeneous tissue layer with the actual correlation length of the abdominal wall is applied to introduce the additional random phase shift. The simulation results are also demonstrated by the experimental measurements with an eight-element transducer array and a phase screen slab. The good agreement between numerical simulations and experimental measurements prove that the phase screen has a more obvious impact on the distribution of acoustic pressure than that of phase. When the thickness variation is less than one wavelength, no significant influence on the generation of AVs can be produced. The variations of vortex nodes and antinodes in terms of the location, shape, and size of AVs are not obvious. Although the circular pressure distribution might be deformed by the thickness variation larger than one wavelength, AVs can still be generated around the beam axis with perfect phase spirals. The favorable results certify the feasibility of AV generation inside the human body and suggest the application potential of multiple traps in object manipulation.

2. Principle and method

To generate the AV beam at the frequency of MHz in water, the phase-coded approach is employed to excite the N-element circular transducer array, which is illustrated in Fig. 1. N planar piston transducers (radius a) are fixed uniformly on a circumference (radius R) with a spatial angle difference of $\Delta\varphi = 2\pi/N$[12–15] to form a circular source plane. N sinusoidal signals at the angular frequency ω are used to drive the transducers to produce the composite acoustic beam in free space above the source plane. The phase difference between the adjacent sources is set to $\Delta\phi = l\Delta\varphi$ to generate the AV beam with a controllable topological charge l. If the radius a is not much less or even bigger than the wavelength of the acoustic waves, the radiation pattern $D(\theta) = |2\mathrm{J}_1(ka\sin\theta)/(ka\sin\theta)|$[12–15] of the transducers should be considered, where $\mathrm{J}_1(x)$ is the Bessel function of first order, θ is the radiation angle of the source, $ka = \omega a/c$ is the key factor determining the radiation directivity of the planar transducer, and $k = \omega/c$ is the wave number for the acoustic velocity c.

By setting the center of the source plane as the origin in the cylindrical coordinates as shown in Fig. 1, the position and the initial phase of the n-th source S_n can be expressed as $(R, \varphi_{0n}, 0)$ and ϕ_{0n} for $\varphi_{0n} = (n-1)\Delta\varphi$ and $\phi_{0n} = (n-1)\Delta\phi$. The acoustic pressure[15] transmitted from S_n to the observation position Q at (r, φ, z) can be written as

$$p_n(r,\varphi,z) = \mathrm{j}\omega\frac{\rho_0 u_0 a^2}{R_n}\left[\frac{\mathrm{J}_1(ka\sin\theta)}{ka\sin\theta}\right] \times \exp[\mathrm{j}(\omega t - kR_n)]\exp(\mathrm{j}\phi_{0n}), \quad (1)$$

where u_0 is the vibration velocity amplitude of the source surface, and ρ_0 is the density of the medium.

$$R_n = \sqrt{(r\cos\varphi - R\cos\varphi_{0n})^2 + (r\sin\varphi - R\sin\varphi_{0n})^2 + z^2}$$

is the propagation distance from S_n to Q, and $\theta = \arcsin\left(\sqrt{R_n^2 - z^2}/R_n\right)$. Then, in order to generate AVs, the phase difference $\Delta\phi = 2\pi l/N$ is used to produce a total phase shift of $2\pi l$ for the N sources. Therefore, by considering φ_{0n} and ϕ_{0n} for each source, the acoustic pressure at Q can be calculated as the summation of all the transmitted signals as

$$p(r,\varphi,z) = \mathrm{j}\omega\rho_0 u_0 a^2 \sum_{n=1}^{N}\left\{\left[\frac{\mathrm{J}_1(ka\sin\theta)}{R_n ka\sin\theta}\right] \times \exp[\mathrm{j}(\omega t - kR_n)]\exp[\mathrm{j}\phi_{0n}]\right\}. \quad (2)$$

It can be observed that the radiation pattern of each source is determined by ka. For $ka \ll 1$, $D(\theta) = |2J_1(ka\sin\theta)/(ka\sin\theta)|$ can be simplified to 1 and the transducer can be treated as a point source to generate a spherical radiation. Due to the circular symmetry of the sources with a fixed phase difference in turn, the generation of AVs from the source plane along the central axis has been demonstrated.[15,24] However, with the increase of ka, the directivity of the acoustic beam appears with obvious side lobes and the corresponding pressure nulls (PNs). For the transducers with $ka \gg 1$, the sketch map of the axial profile for the generation of AVs is illustrated in Fig. 1(b) without the inserted tissue layer. It shows that, besides the AV generated by the main lobes of the sources, cone-shaped AVs produced by the side lobes are closer to the source plane with relatively lower pressures. Corresponding to the radiation angles of the PNs between the lobes, several vortex valleys (nodes) with nearly pressure zero can be generated on the central axis to form multiple Gor'kov potential traps.[15] For a fixed ka, the axial distances of vortex nodes can be calculated by $R/\tan\theta$, where θ is the radiation angle of PN determined by the roots of $\mathrm{J}_1(ka\sin\theta)$. Hence, the number and position of vortex nodes on the beam axis can be predicted, which is beneficial to the precise design of deep-level multiple traps.

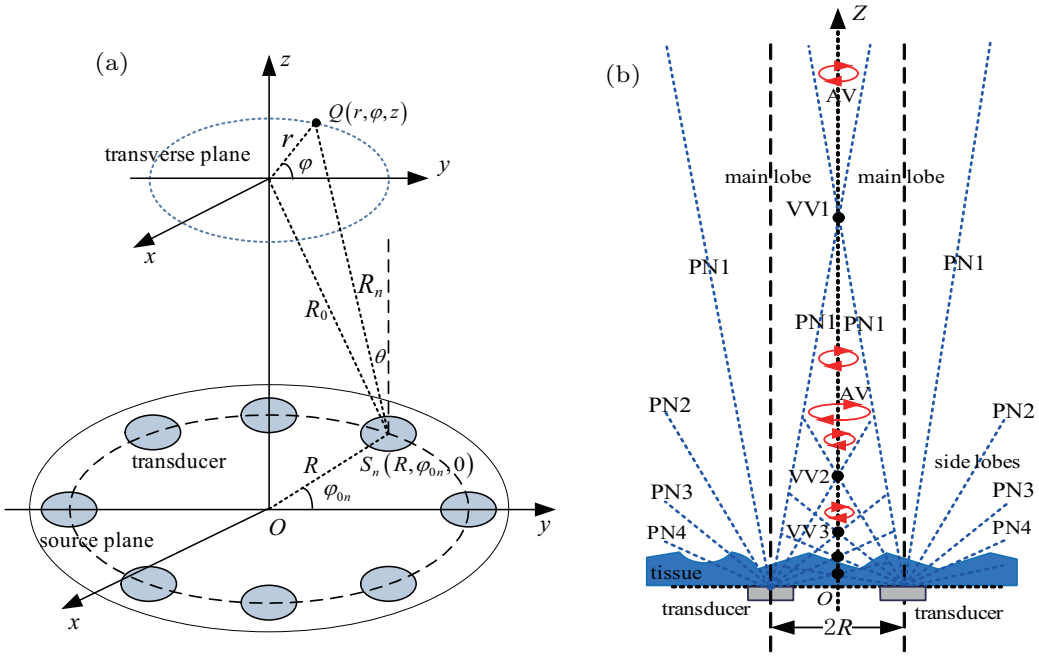


Fig. 1. (color online) (a) Schematic diagram of the AV generation system with the N-element circular transducer array, and (b) the sketch map of the axial profile with the insertion of an inhomogeneous tissue layer.

Although the multiple traps of the AV beam along the center axis can be generated by the main lobe and the side lobes in water, they are also influenced by the complex structure of the abdominal wall with obvious inhomogeneity. Through one-dimensional (1-D) fluctuation measurement of time delay for the abdominal wall, Krammer[25] observed that the arrival time of the wave front was different from each other with random individual difference. The time delay followed the statistic law[26] with a correlation length of 2–10 mm. Hinkelman[27] demonstrated that the time-shift aberration formed by the abdominal wall could be explained by the simplified phase screen model,[28] and could be estimated by a time-shift compensation algorithm. The inhomogeneous tissue layer can be regarded as a thin layer for acoustic transmission, and the random phase fluctuation of acoustic wave is only affected by the influence of the acoustic velocity, while

the pressure attenuation is considered as a constant. Based on the correlation length and the mean square deviation (standard deviation) parameter,[21,22] the phase screen is generated randomly by a two-dimensional (2-D) phase interference data.

By considering the inhomogeneity of a tissue layer, the phase screen is applied to calculate the distribution of acoustic pressure. Assume that the attenuation coefficient and the acoustic speed in tissues are higher than those in water with the differences of $\Delta\alpha$ and Δc, and the transmission distance of the n-th source can be written as $R_n = R_{n\mathrm{W}} + R_{n\mathrm{T}}$, where $R_{n\mathrm{W}}$ and $R_{n\mathrm{T}}$ are the distances in water and in the tissue layer, respectively. The additional acoustic attenuation in the tissue layer can be simplified to $\exp(-\Delta\alpha R_{n\mathrm{T}}) = 1$, and the reduced transmission time can be calculated by $\Delta t = R_{n\mathrm{T}}/(c+\Delta c) - R_{n\mathrm{T}}/c = R_{n\mathrm{T}}\Delta c/[(c+\Delta c)c]$. Therefore, the acoustic pressure in Eq. (2) can be revised to

$$\begin{aligned} & p_{\mathrm{rev}}(r,\varphi,z) \\ &= \mathrm{j}\omega\rho_0 u_0 a^2 \sum_{n=1}^{N} \left\{ \left[\frac{\mathrm{J}_1(ka\sin\theta)}{R_n ka\sin\theta} \right] \right. \\ & \left. \times \exp[\mathrm{j}(\omega t - \omega\Delta t - kR_n)] \exp[\mathrm{j}\phi_{0n}] \right\}. \end{aligned} \tag{3}$$

Hence, the transmission distance $R_{n\mathrm{T}}$ in the tissue layer can be calculated by a geometric method, and the phase shift can be achieved with the thickness variation. The distributions of acoustic pressure and phase before and after the insertion of the phase screen can be calculated to analyze the influence on the generation of AVs.

3. Numerical and experimental studies

According to the parameters of the experimental setup, numerical studies of acoustic pressure and phase of the AV beam with $a = 0.7$ cm, $R = 3$ cm, and $N = 8$ were conducted at $f = 1$ MHz. The phase difference of the adjacent sources was set to $\Delta\phi = \pi/8$ to generate the AV beam with a topological charge of 1. The sound speed in water was $c = 1500$ m/s. For the circular transducers with a high ka of 29.32, the radiation pattern of the sources was considered in pressure superimposition for AV generation. The distributions of AVs before and after the insertion of the phase screen were simulated, and also compared with the experimental results.

The axial pressure profile of the AV beam generated by the transducer array from $z = 10$ cm to 40 cm is illustrated in Fig. 2(a). It is clear that the acoustic pressure along the beam axis is almost zero, indicating the formation of the vortex cores of AVs at different axial distances. Several regions of AVs produced by the main lobe and the side lobes are clearly displayed with obvious pressure nulls produced between the lobes. Compared to the AV generated by the side lobes of the sources, the acoustic pressure of the AV generated by the main lobe is much higher at a longer axial distance. Corresponding to the maximum and minimum pressures of the AV beam around the center axis, obvious vortex nodes and antinodes are distributed alternatively at different axial distances. As shown in Fig. 2(a), two vortex nodes are located at 12 cm and 22 cm, while two antinodes are positioned at 17 cm and 40 cm, respectively.

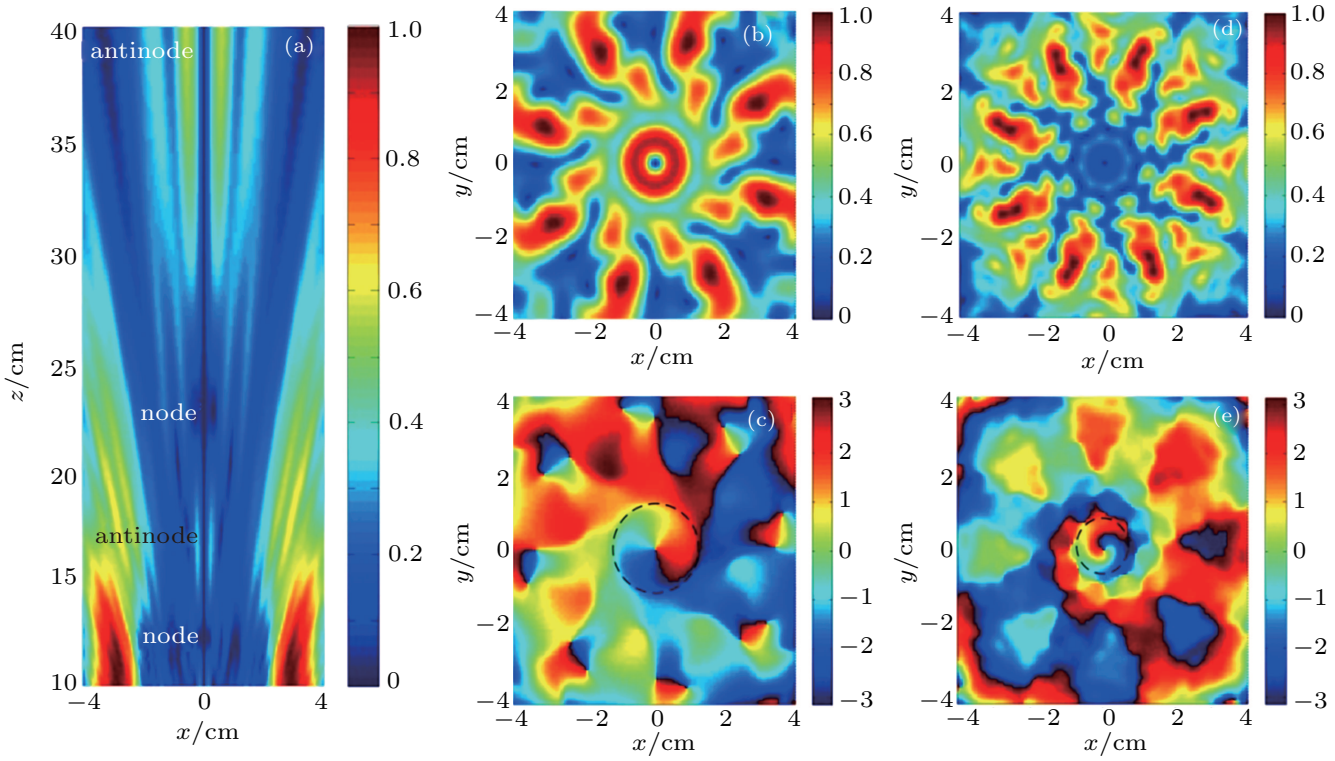


Fig. 2. (color online) Numerical results of (a) the axial pressure profile and the cross-sectional distributions of (b), (d) pressure and (c), (e) phase for the AV beam at the axial distances of (b), (c) 40.0 cm and (d), (e) 22 cm in water.

In order to analyze the characteristics of the vortex antinodes, the cross-sectional distributions of pressure and phase at $z = 40$ cm are plotted in Figs. 2(b) and 2(c). In the center region ($r < 1.0$ cm) in Fig. 2(b), obvious circular distributions with a center pressure zero are clearly displayed, and the radius of the pressure peak is located at $r = 0.8$ cm. The corresponding phase distribution in Fig. 2(b) shows a perfect phase spiral around the vortex center with a singularity at the origin, demonstrating the formation of the AV. Meanwhile, although the acoustic pressure is influenced by the eight sources as shown in Fig. 2(a), an expanded scope with complete phase spiral in $r < 1.2$ cm (dashed circle) indicates the existence of an effective AV. As a comparison to vortex antinodes, the cross-sectional distributions of pressure and phase at $z = 22$ cm (vortex node) are plotted in Figs. 2(d) and 2(e). Even though the acoustic pressure in the center region is much lower than that of the surrounding area, an approximately circular distribution can still be observed in Fig. 2(d) and the formation of the AV is also proved by the perfect phase spiral in $r < 0.8$ cm (dashed circle) in Fig. 2(e). Thus, it can be concluded that AVs can be generated along the center axis of the acoustic beam at all the distances. The pressure peaks of the vortex antinodes are much higher than those of the vortex nodes, which can be applied to achieve faster trapping[15] with higher pressure gradient in object manipulation.

It was also reported by Hinkelman[27] that the body wall played the most important role among all the phase fluctuations introduced by the inhomogeneity inside the human body. The spatial distribution of the phase screen was determined by the correlation length, which was the inhomogeneous length scale of tissues. Liu[22] also observed that the inhomogeneity of human tissues had a certain impact on the distribution of a focused ultrasound, while the influence of the correlation length was relatively small. Therefore, in this study, an inhomogeneous tissue layer with a correlation length of 3.0 mm and a controllable thickness variation was used to investigate the influence on the generation of AVs. In numerical studies, a phase screen model is used to depict the extended random medium with a series of slabs at a random thickness. The phase variation can be calculated by the fluctuation of the random thickness introduced time-shift. When the thickness is the order of the correlation length of the inhomogeneous tissue layer, the random phase variation is produced by the projection onto a screen without the consideration of acoustic attenuation, which exhibits a Gaussian correlation function with a zero mean. The simulation model of the phase screen with the maximum thickness variation of one wavelength ($\pm\lambda/2$) is shown in Fig. 3(a), which is assumed to be placed in front of the transducer array to produce the random phase interference.

By considering the time-shift of the thickness variation, the pressure distribution was simulated with the insertion of the inhomogeneous tissue layer based on Eq. (3). The axial pressure profile from $z = 10$ cm to 40 cm presented in Fig. 4(a) shows a consistent distribution to Fig. 2(a) with an approximately symmetric structure. The acoustic pressure on the beam axis is much lower than that at the surrounding area, and several vortex nodes and antinodes along the beam axis can also be observed at similar axial distances. However, due to the influence of the random time-shift of phase variation, the pressure distribution is deformed significantly with an asymmetry in pressure amplitude, especially for the vortex nodes and antinodes in terms of the location, shape, and size around the beam axis.

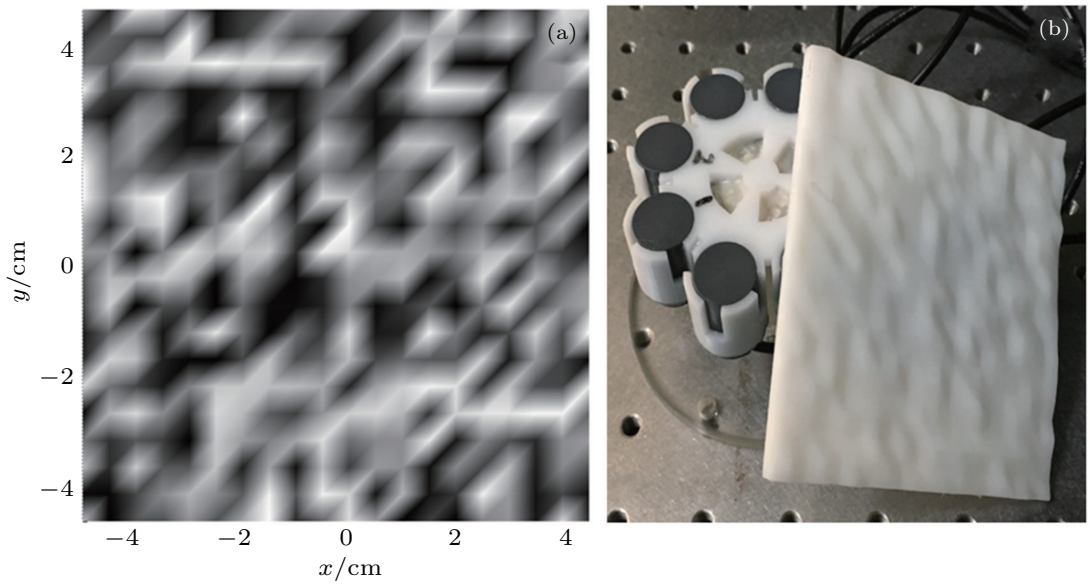


Fig. 3. (a) Simulation model of the random phase screen, and (b) the picture of the experimental transducer array and the fabricated inhomogeneous tissue layer with the thickness of (4 ± 0.75) mm.

For the vortex antinode at $z = 40$ cm in the transverse plane, the acoustic pressure at the origin is almost zero as shown in Fig. 4(b), and an approximate circular distribution can still be identified with the pressure peaks located at $r = 0.5$ cm. Meanwhile, the corresponding distribution of phase in Fig. 4(c) shows a perfect spiral around the origin in $r < 0.7$ cm (dashed circle) and a less perfect spiral in 0.7 cm$< r < 1.2$ cm (dashed circle), still demonstrating the formation of the AV in the transverse plane. In addition, for the vortex node at $z = 22$ cm, although the acoustic pressure in the center region is very low in Fig. 4(d), the circular pressure distribution with a perfect phase spiral in $r < 0.5$ cm (dashed circle) in Fig. 4(d) also proves the existence of the AV. The simulation results indicate that, for the random phase screen with the maximum thickness variation in one wavelength, AVs can be generated along the beam axis at all the distances with a reduced effective radius. With the increase of the thickness variation range, more significant impact on the formation of AVs can be produced by the greater phase shifts, which are introduced by the bigger thickness variations of the inhomogeneous tissue layer.

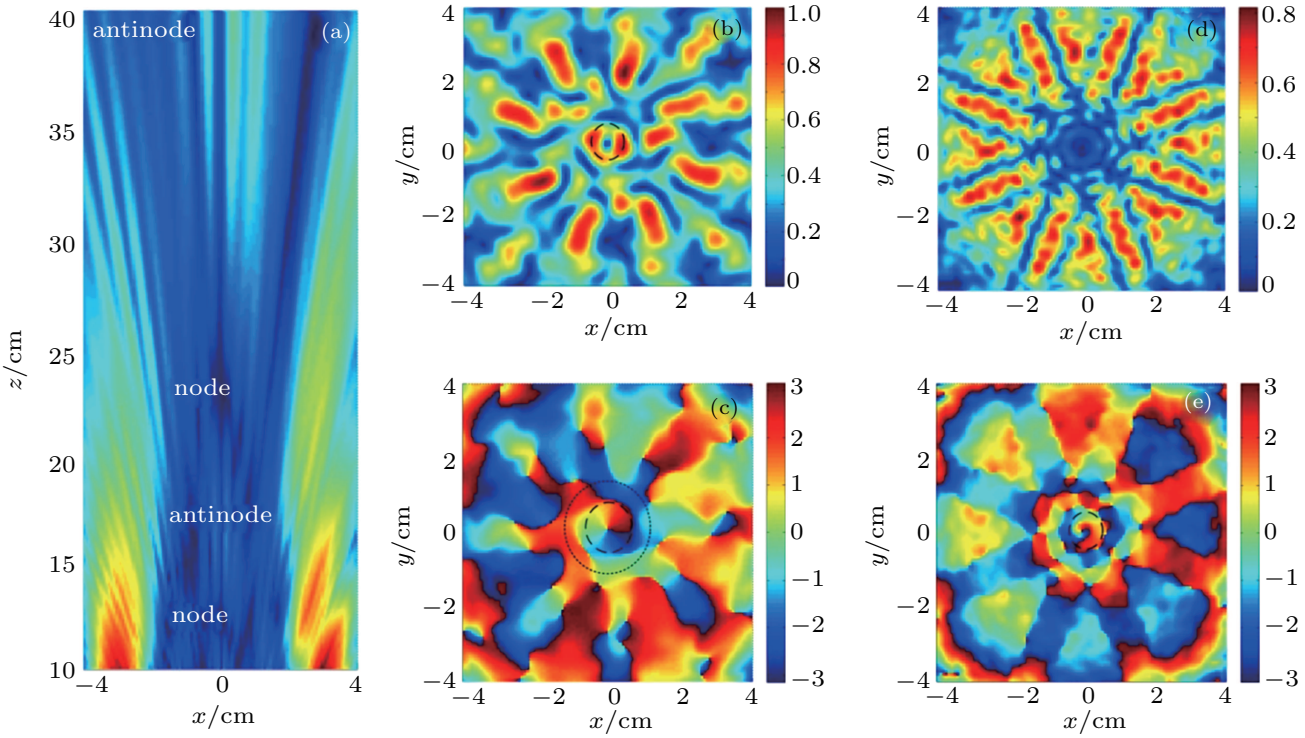


Fig. 4. (color online) Numerical results of (a) the axial pressure profile and the cross-sectional distributions of (b), (d) pressure and (c), (e) phase for the AV beam at the axial distances of (b), (c) 40 cm and (d), (e) 22 cm with the insertion of the inhomogeneous tissue layer.

According to the parameters of the simulation model in Fig. 3(a), an inhomogeneous tissue layer as shown in Fig. 3(b) was fabricated by a photopolymer (ZR820 RESIN, acoustic speed 2540 m/s) using the 3-D printing technology. The maximal and minimal thicknesses of the slab were set from 3.25 mm to 4.75 mm with the variation range of one wavelength. The experimental transducer array as shown in Fig. 3(b) was assembled by eight planar position transducers ($a = 0.7$ cm) fixed on a circumference ($R = 3$ cm) on an acrylic plane. An eight-channel phase-coded device[15] made of DDS chips and power amplifiers was applied to drive the transducers. Then, with the 3-D scanning system (Newport M-ILS250, Newport Corporation, USA), the distribution of the acoustic field was measured by a needle hydrophone (Onda HNR-1000, Onda Corporation, USA). The step grid of the measurements was set to 0.8 mm. The radial distance was set to 8 cm for the x and y directions, and the axial distance was set from 10 cm to 40 cm.

With the insertion of the tissue layer, the experimental axial pressure profile illustrated in Fig. 5(a) agrees well with the simulation result in Fig. 4(a). A basically symmetrical distribution is clearly displayed with almost pressure zero along the beam axis. The vortex nodes and antinodes can also be visualized at the axial distances around 12 cm, 17 cm, 22 cm, and 40 cm. However, the symmetrical pressure distribution is deformed by the influence of the phase screen. The location, shape, and size of vortex nodes and antinodes are not exactly the same as those in Fig. 4(a), which are also too vague to be differentiated clearly. Corresponding to Figs. 4(b) and 4(e), the cross-sectional measurements were conducted at $z = 40$ cm and 22 cm, which are plotted in Figs. 5(b)–5(e). For the vortex antinode at $z = 40$ cm as shown in Fig. 5(b), a clear pressure zero is clearly displayed at the origin. Except for the pressure peaks at $r = 0.8$ cm (dashed circle), the circular pressure distribution around the vortex center cannot be formed,

whereas, the perfect phase spiral in $r < 0.9$ cm (dashed circle) displayed in Fig. 5(c) also demonstrates the existence of the AV. In addition, for the vortex node at $z = 22$ cm as shown in Fig. 5(d), the distribution in the center region is in a mess at a low-level pressure and the influence of the sources cannot be identified clearly. Nevertheless, the formation of the AV can still be demonstrated by the perfect phase spiral in $r < 0.5$ cm (dashed circle) in Fig. 5(e). Thus, the experimental results provide further evidence to the lesser influence of the phase screen on the generation of AVs.

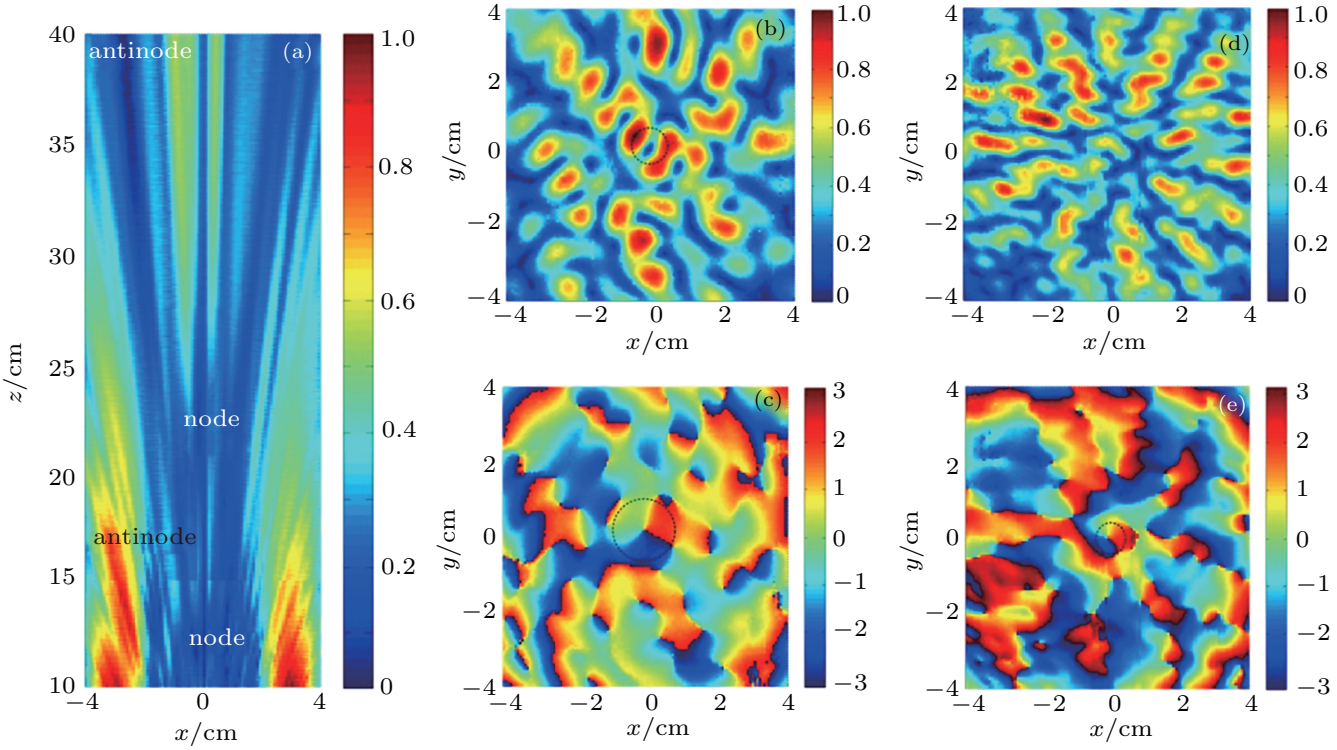


Fig. 5. (color online) Experimental results of (a) the axial pressure profile and the cross-sectional distributions of (b), (d) pressure and (c), (e) phase of the AV beam at the axial distances of (b), (c) 40 cm and (d), (e) 22 cm with the inhomogeneous tissue layer.

4. Discussion

The phase screen model used in this study is an efficient approximation method to deal with the influence of random media on wave propagation, providing a clear physical concept for phase interference. The model separates the influences of amplitude attenuation and phase shift from each other to realize theoretical simplification. For the acoustic transmission through an actual inhomogeneous tissue layer, the impact of the random phase screen on the acoustic pressure and phase can be produced by the difference of the thickness. With the random phase screen, the variation of acoustic attenuation is not obvious, while the phase change caused by the acoustic speed is relatively significant with an intensive phase fluctuation. The generation of AVs with the circular transducer array is the superimposition result of the phased acoustic beams, which is more sensitive to the phase variations of the radiated waves. Thus, the random phase screen model is sufficient to analyze the influence of the tissue layer on the generation of AVs inside human body. However, by considering the effects of the acoustic attenuation and the phase shift of the abdominal wall, more accurate study should be further carried out, which shows its great significance to the practical application of AVs in biomedical engineering.

Also as we know, the cross section of an ideal AV has a circular pressure distribution and a helical phase distribution. The time-averaged flux of the OAM density around each circumference in the transverse plane is the same with a same circular distribution of the acoustic radiation force, which is beneficial for the accurate design of particle manipulation. Although the ideal circular pressure distribution might be deformed by the influence of the phase screen with random phase shifts, the formation of AVs can also be proved by the helical phase distributions. The effects of object manipulation and particle accumulation can still be realized by the helical direction of the acoustic radiation forces around each circumference, in spite of the difference of OAMs. Moreover, in order to reduce the influence of the inhomogeneous abdominal wall, a lower frequency of acoustic signals with a bigger wavelength should be applied to achieve the relatively smaller phase differences of the random phase screen. The deformation of AVs introduced by the phase screen can also be reduced by the cancellation effect of phase interference for more acoustic sources of the circular array.

The experimental measurements exhibit good agreements

with the numerical results, demonstrating the formation of AVs along the beam axis before and after the insertion of the inhomogeneous tissue layer. However, obvious differences can still be observed between the experimental and theoretical results, which might be introduced by the uncertain factors as below. Firstly, the error is produced probably by the asymmetric structure of the transducer array and the inconsistency of the sources. Secondly, since the results are influenced by the randomness of the inhomogeneous tissue layer, the acoustic distribution of each experimental measurement is unique, which is different from the others. In addition, further investigations on the correlation length impact of the tissue layer and the optimization algorithm[29] of the random phase screen should also be performed for AVs in the practical application of biological tissues.

5. Conclusion

In this paper, based on the acoustic radiation of a circular array of planar piston sources, the mechanism underlying the generation of AVs is investigated with the consideration of the random phase screen. By applying the actual parameters of the abdominal wall, numerical simulations before and after the insertion of the inhomogeneous tissue layer are performed, and also demonstrated by experimental measurements. Both theoretical and experimental results prove that the distribution of AVs can be affected by the phase screen with random time-shifts. In the actual thickness variation range of human tissues, no obvious influence of the phase screen can be introduced to the generation of AVs, and the variations of vortex nodes and antinodes in terms of the location, shape, and size are not significant. Although the circular pressure distribution might be deformed by the phase interference with the thickness variation higher than one wavelength, AVs can still be generated with perfect phase spirals around the center axis with a reduced effective radius. The favorable results provide the feasibility of the generation of AVs through the abdominal wall, and suggest the application potential of object manipulation inside the human body in biomedical engineering.

References

[1] Nye J F and Berry M V 1974 *Proc. R. Soc. Lond. A* **336** 165
[2] Allen L, Beijersbergen M W, Spreeuw R J, *et al.* 1992 *Phys. Rev. A* **45** 8185
[3] Neuman K C and Block S M 2004 *Rev. Sci. Instr.* **75** 2787
[4] Hoshi T, Ochiai Y and Rekimoto J 2014 *Jpn. J. Appl. Phys.* **53** 07KE07
[5] Li F, Cai F, Liu Z, *et al.* 2014 *Phys. Rev. Appl.* **1** 051001
[6] Broadbent E G and Moore D W 1979 *Royal Society* **290** 353
[7] Lekner J 2007 *Phys. Rev. E* **75** 036610
[8] Torabi R and Rezaei Z 2013 *Phys. Lett. A* **377** 1668
[9] Hefner B T and Marston P L 1999 *J. Acoust. Soc. Am.* **106** 3313
[10] Anhäuser A, Wunenburger R and Brasselet E 2012 *Phys. Rev. Lett.* **109** 034301
[11] Demore C E M, Zhengyi Y, Alexander V, *et al*. 2012 *Phys. Rev. Lett.* **108** 194301
[12] Yang L, Ma Q, Tu J, *et al*. 2013 *J. Appl. Phys.* **113** 154904
[13] Gao L, Zheng H, Ma Q, *et al*. 2014 *J. Appl. Phys.* **116** 024905
[14] Zheng H, Gao L, Ma Q, *et al*. 2014 *J. Appl. Phys.* **115** 084909
[15] Li Y, Guo G, Ma Q, *et al*. 2017 *J. Appl. Phys.* **121** 164901
[16] Amin V, Ron Roberts R, Long T, *et al*. 2006 *AIP Conf. Proc.* **829** 201
[17] Xue H, Liu X Z, Gong X F and Zhang D 2005 *Acta Phys. Sin.* **54** 5233 (in Chinese)
[18] Liu X, Li J, Chang Y, *et al*. 2007 *Phys. Lett. A* **362** 50
[19] Liu D and Waag R 1997 *J. Acoust. Soc. Am.* **101** 1172
[20] Uscinski B J, Macaskill J C, Ewart T E 1983 *J. Acoust. Soc. Am.* **74** 1474
[21] Liu Z, Fan T, Guo X, *et al*. 2010 *Chin. Phys. Lett.* **27** 094303
[22] Liu Z, Fan T, Zhang D, *et al*. 2009 *Chin. Phys. B* **18** 4932
[23] Mast T D, Hinkelman L M, Orr M J, *et al.* 1997 *J. Acoust. Soc. Am.* **102** 1177
[24] Volke-Sepúlveda K, Santillán A O and Boullosa R R 2008 *Phys. Rev. Lett.* **100** 024302
[25] Krammer P and Hassler D 1987 *Proc. IEEE Ultrason. Symp.* 939
[26] Sumino Y and Waag R C 1991 *J. Acoust. Soc. Am.* **90** 2924
[27] Mast T D, Hinkelman L, Orr M J, *et al.* 1998 *J. Acoust. Soc. Am.* **104** 3651
[28] Uscinski B J 1997 *The Elements of Wave Propagation in Random Media* (New York: McGraw-Hill)
[29] Shao W and Xian H 2016 *Chin. Phys. B* **25** 114212